

Global stratospheric temperature changes

1 **Isolating the roles of different forcing agents in global stratospheric temperature**
2 **changes using model integrations with incrementally added single forcings.**

3 V. Aquila^{1,2,3}, W. H. Swartz⁴, D. W. Waugh², P. R. Colarco³, S. Pawson⁵, L. M. Polvani⁶,
4 R. S. Stolarski²

5 ¹Goddard Earth Science Technology & Research (GESTAR), Columbia, MD

6 ²Johns Hopkins University, Department of Earth and Planetary Science, Baltimore, MD

7 ³Laboratory for Atmospheric Chemistry and Dynamics (Code 614), NASA Goddard Space
8 Flight Center, Greenbelt, MD

9 ⁴Johns Hopkins University Applied Physics Laboratory, Laurel, MD

10 ⁵Global Modeling and Assimilation Office, NASA Goddard Space Flight Center,
11 Greenbelt, MD

12 ⁶Columbia University, New York, NY

13 Manuscript prepared for Journal of Geophysical Research, second revision

14 Version: 4 April 2017

15 **Key points:**

16 ODS cooled the stratosphere only up to the mid 1990s.

17 GHGs are the driver of the middle and upper stratospheric cooling since 2000

18 The stair-step pattern in temperature is due to a combination of all forcings

19

20

21 **Abstract**

22 Satellite instruments show a cooling of global stratospheric temperatures over the whole
23 data record (1979-2014). This cooling is not linear, and includes two descending steps in
24 the early 1980s and mid-1990s. The 1979-1995 period is characterized by increasing
25 concentrations of ozone depleting substances (ODS) and by the two major volcanic
26 eruptions of El Chichón (1982) and Mount Pinatubo (1991). The 1995-present period is
27 characterized by decreasing ODS concentrations and by the absence of major volcanic
28 eruptions. Greenhouse gas (GHG) concentrations increase over the whole time period. In
29 order to isolate the roles of different forcing agents in the global stratospheric temperature
30 changes, we performed a set of AMIP-style simulations using the NASA Goddard Earth
31 Observing System Chemistry-Climate Model (GEOSCCM). We find that in our model
32 simulations the cooling of the stratosphere from 1979 to present is mostly driven by
33 changes in GHG concentrations in the middle and upper stratosphere and by GHG and
34 ODS changes in the lower stratosphere. While the cooling trend caused by increasing
35 GHGs is roughly constant over the satellite era, changing ODS concentrations cause a
36 significant stratospheric cooling only up to the mid-1990s, when they start to decrease
37 because of the implementation of the Montreal Protocol. Sporadic volcanic events and the
38 solar cycle have a distinct signature in the time series of stratospheric temperature
39 anomalies but do not play a statistically significant role in the long-term trends from 1979
40 to 2014. Several factors combine to produce the step-like behavior in the stratospheric
41 temperatures: in the lower stratosphere, the flattening starting in the mid 1990's is due to
42 the decrease in ozone depleting substances; Mount Pinatubo and the solar cycle cause the
43 abrupt steps through the aerosol-associated warming and the volcanically induced ozone
44 depletion. In the middle and upper stratosphere, changes in solar irradiance are largely

45 responsible for the step-like behavior of global temperatures anomalies, together with
46 volcanically induced ozone depletion and water vapor increases in the post-Pinatubo years.

47 **1.INTRODUCTION**

48 Since the beginning of the 1980s, global stratospheric temperatures have decreased at all
49 altitudes (*e.g. Seidel et al., 2011*). This cooling includes two abrupt steps coincident with
50 the major volcanic eruptions of El Chichón and Mount Pinatubo in 1982 and 1991,
51 respectively (*Pawson et al., 1998*). There has not been any significant cooling of the global
52 lower stratosphere since 1995, while in the middle and upper stratosphere the cooling has
53 resumed after a pause that lasted from the mid-1990s to the mid-2000s (*McLandress et al.,*
54 *2015*).

55 Prior studies have shown that increases in concentrations of anthropogenic greenhouse
56 gases (GHGs) and ozone-depleting substances (ODSs) have driven a sustained cooling of
57 the stratosphere since 1980 (*e.g. Ramaswamy and Schwarzkopf, 2002; Santer et al., 2003;*
58 *Shepherd and Jonsson, 2008; Thompson and Solomon, 2009; Stolarski et al., 2010*). The
59 natural forcing by the solar cycle and occasional volcanic eruptions also impacted the
60 temporal behavior of global stratospheric temperatures. The solar cycle affected
61 stratospheric temperatures directly, via changes in incoming radiation, and indirectly, by
62 modulating ozone formation and destruction (*Gray et al., 2009; Swartz et al., 2012*);
63 volcanic sulfate aerosols warmed the stratosphere by absorbing long-wave and near-
64 infrared radiation (*Angell, 1997*). In a high-chlorine atmosphere, volcanic aerosols also
65 enhanced stratospheric ozone depletion (*Tie and Brasseur, 1995*), thereby cooling the
66 stratosphere. Ozone depletion following the Mt. Pinatubo eruption caused a negative

Global stratospheric temperature changes

67 temperature anomaly in the lower stratosphere that persisted after the warming effect of
68 the aerosol dissipated (*Thompson and Solomon, 2009*).

69 Here, we analyze the changes in stratospheric temperatures from 1979 to 2014 using
70 satellite observations and model simulations. We examine the temperature retrievals from
71 the Tiros Operational Vertical Sounder (TOVS) Microwave Sounding Unit (MSU) dataset
72 in the lower stratosphere (*Mears and Wentz, 2009*) and the Advanced Microwave Sounding
73 Unit (AMSU) and Stratospheric Sounding Unit (SSU) merged dataset in the middle and
74 upper stratosphere (*McLandress et al., 2015*), together with simulations using a version of
75 the NASA Goddard Earth Observing System Chemistry-Climate Model (GEOSCCM,
76 *Oman and Douglass, 2014*) that includes a prognostic scheme for aerosol and a
77 comprehensive stratospheric chemistry module. A systematic suite of simulations is
78 performed to isolate the individual and combined impacts of GHGs, ODS, changes in solar
79 radiation, and volcanic aerosols on the complex temporal changes in global-mean
80 stratospheric temperatures.

81 Previous modeling studies have investigated the impacts of different forcings on
82 stratospheric temperatures (*e.g. Ramaswamy and Schwarzkopf, 2002; Jones et al., 2003;*
83 *Ramaswamy et al., 2006; Shepherd and Jonsson, 2008; Stolarski et al., 2010; Gillett et al.,*
84 *2011; Santer et al., 2013*), but they mostly focused on the lower stratosphere or analyzed
85 the role of only some of the forcing agents, for instance ODS versus GHGs, or
86 anthropogenic versus natural forcings. This is the first study to provide a systematic and
87 comprehensive analysis of the role of each of GHGs, ODSs, solar irradiance, and volcanic
88 aerosol on the global temperatures in the lower, middle, and upper stratosphere.

89 Furthermore, this study is the first stratospheric temperature analysis to include two whole
90 decades of observations (1995-2014) free of major volcanic eruptions. This volcanically
91 quiescent period facilitates the estimation of the 11-year solar component of stratospheric
92 temperature change. These last two decades are also long enough to allow for the
93 calculation of temperature trends in an atmosphere characterized by decreasing ODS
94 concentrations.

95 A description of the observational data record, the climate model and the simulation setup
96 is included in Section 2. Section 3 contains the results of this study: Sections 3.1 and 3.2
97 explain the role played by the different forcing agents on the changes of the time-series of
98 global stratospheric temperature, while Section 3.3 focuses on global stratospheric
99 temperature trends.

100 **2. OBSERVATIONS AND MODEL SIMULATIONS**

101 **2.1 DESCRIPTION OF THE DATA RECORDS**

102 The NOAA Microwave Sounding Units (MSU) and Advanced Microwave Sounding Units
103 (AMSU) have provided measurements of stratospheric temperatures starting from
104 December 1978. The observed lower stratospheric anomalies are here calculated from the
105 Remote Sensing System (RSS) data record (*Mears and Wentz, 2009*), which covers the 15-
106 20 km altitude range and merges measurements from MSU channel 4 from late 1978 to the
107 early 2000s and from AMSU channel 9 after 1998.

108 In the middle and upper stratosphere, we use temperature anomalies computed from the
109 *McLandress et al. (2015)* dataset, which merges the SSU and AMSU temperature records.
110 SSUs operated onboard NOAA satellites from 1979 to 2006 and provided estimates of

111 near-global (75°S-75°N) temperature changes. *McLandress et al.* (2015) created a
112 continuous stratospheric temperature dataset from 1979 to 2012 for the middle and upper
113 stratosphere. They transformed AMSU temperature data using the SSU 1, 2, and 3
114 weighting functions, which span the altitude ranges from 25km to 35 km, 35 km to 45 km,
115 and 40 km to 50 km, respectively (*Randel et al.*, 2009). Between 1979 and 2006,
116 *McLandress et al.* (2015) used the bias-corrected and cross-calibrated time series of SSU
117 radiances by *Zou et al.* (2014). The *Zou et al.* (2014) dataset is an update from the previous
118 NOAA STAR SSU stratospheric temperature record (*Wang et al.* 2012), which showed
119 large discrepancies relative to the UK Met Office SSU temperature record independently
120 produced by *Nash and Forrester* (1986) (*Thompson et al.*, 2012). The UK Met Office
121 temperature record has also been recently reprocessed by *Nash and Saunders* (2015) and
122 is now in good agreement with the *Zou et al.* (2014) temperature dataset.

123 All temperature anomalies shown here are calculated using the near-global time series of
124 observed lower stratospheric temperatures with respect to the January 1995-December
125 2011 period. This reference period is chosen because it is the longest period in the
126 combined MSU/AMSU/SSU data record free of major volcanic perturbations.

127 **2.2 DESCRIPTION OF THE CLIMATE MODEL AND EXPERIMENT SETUP**

128 GEOSCCM is an aerosol and chemistry focused version of the GEOS-5 Earth system
129 model, including radiatively and chemically coupled tropospheric and stratospheric aerosol
130 and atmospheric chemistry. GEOSCCM couples the GEOS-5 atmospheric general
131 circulation model (*Rienecker et al.*, 2008; *Molod et al.*, 2012) to the comprehensive
132 stratospheric chemistry module StratChem (*Pawson et al.*, 2008), and the Goddard
133 Chemistry, Aerosol, Radiation, and Transport Model (GOCART, *Chin et al.*, 2000;

134 *Colarco et al.*, 2010). GOCART is a bulk aerosol model with components for dust, sea salt,
135 black carbon, organic carbon, and sulfate aerosol. Versions of GEOSCCM that include
136 StratChem have been evaluated in the two phases of the Chemistry-Climate Model
137 Validation (CCMVal; *Eyring et al.*, 2006; *SPARC*, 2010) and reliably simulate the
138 stratospheric circulation and transport of trace gas species and many key features of
139 observed stratospheric chemistry, such as polar ozone depletion (*Strahan et al.*, 2011;
140 *Douglass et al.* 2012).

141 The version of GEOSCCM used in this work (*Oman and Douglass*, 2014) includes several
142 advances, among which are a parameterization of gravity waves that can force a quasi-
143 biennial oscillation with realistic features and a new air/sea roughness parameterization
144 that leads to a more realistic climate (*Molod et al.*, 2012). From a chemical perspective,
145 an additional 5 ppt of CH₃Br has been added to the surface mixing ratios prescribed in the
146 halogen scenario used for CCMVal, to represent very short-lived brominated substances
147 (*Liang et al.*, 2010). For this study, we also included the effects of the solar cycle in total
148 and spectral irradiance on atmospheric heating and photolysis, as implemented by *Swartz*
149 *et al.* (2012). Volcanic eruptions are simulated as a direct injection of sulfur dioxide (SO₂).
150 The subsequent transformation of the sulfur dioxide into sulfate aerosol, its atmospheric
151 transport, and its perturbation of atmospheric chemistry and radiation are interactively
152 calculated within the model. The transport of the aerosols from the Mt. Pinatubo eruption
153 and their effects on ozone have been studied in GEOSCCM by *Aquila et al.* (2012; 2013).
154 The simulations performed in this study span the period from January 1960 to December
155 2014. Here we focus on the satellite era and show results from 1979 to 2014. Each
156 experiment is composed of three ensemble members initialized with different initial

Global stratospheric temperature changes

157 conditions from a 1960 time-slice simulation. All simulations use prescribed sea surface
158 temperatures (SSTs) and sea ice concentrations from the MetOffice Hadley Centre
159 observational dataset (*Rayner et al, 2006*), and emissions of tropospheric aerosol and
160 aerosol precursors following *Granier et al. (2011)*. External forcings are added sequentially
161 (see Table 1). The following experiments are performed:

- 162 • SST, which uses time-varying observed SSTs for the whole simulated period and
163 prescribed concentrations of GHGs and ODS fixed at 1960-levels. Volcanic
164 eruptions are not explicitly included in this experiment, and the solar forcing is held
165 constant;
- 166 • +GHG, which includes observed SSTs and increasing GHG concentrations (Fig.
167 1a). GHG concentrations are from observations up to 2005 and from the
168 Representative Concentrations Pathway 4.5 after 2005 (*Meinhausen et al., 2011*);
- 169 • +ODS, which includes observed SSTs, increasing GHGs, and changing ODS
170 concentrations following *WMO (2010)* (Fig. 1b);
- 171 • +Volc, which includes observed SSTs, increasing GHGs, changing ODS, and the
172 SO₂ injected by volcanic eruptions, specified after *Diehl et al. (2012)* up to
173 December 2010 and *Carn et al. (2015)* from January 2011 to December 2014 (Fig.
174 1c). These databases include the magnitude and altitude of the volcanic SO₂
175 injections for each volcanic event;
- 176 • +Sun, which includes observed SSTs, increasing GHGs, changing ODS, volcanic
177 eruptions and changes in solar flux as in *Lean (2000)* and subsequent updates by
178 *Coddington et al. (2015)* (Fig. 1d).

179 We prescribe ODS concentrations and let GEOSCCM calculate the ozone chemistry, rather
180 than prescribing ozone concentrations. A disadvantage of using prognostic stratospheric
181 ozone is that biases in stratospheric temperatures would affect reaction rates, which would,
182 in turn, affects stratospheric temperatures. On the other hand, prescribing ODS
183 concentrations also allows for a better separation of the natural and anthropogenic changes
184 in ozone concentrations, since volcanic aerosols lead to ozone depletion in a high-chlorine
185 atmosphere (*Tie and Brasseur, 1995*). Additionally, ODSs also act as greenhouse gases
186 and lead to additional cooling in the stratosphere

187 The use of prescribed observed SSTs, rather than internally calculated by the model, aliases
188 the effects of all forcings in the simulations, because observed SSTs include the imprint of
189 perturbations such as volcanic eruptions (*Santer et al., 2015*). However, this approach
190 produces a climate state closer to the observed one and restricts attention to intrinsic
191 atmospheric variability, reducing the amplitude of variability between individual
192 realizations.

193 **3. RESULTS**

194 **3.1 TEMPERATURE CHANGES IN THE LOWER STRATOSPHERE**

195 Lower stratospheric temperature changes in MSU/AMSU observations and simulations are
196 shown in Fig. 2. The simulated atmospheric temperatures are weighted using the
197 appropriate MSU lower stratospheric weighting function (*Randel et al., 2009*). Fig. 3
198 displays similar information, along with ozone and water concentrations at 70 hPa, but
199 expressed as the ensemble mean differences between successive pairs of simulations, *e.g.*,

Global stratospheric temperature changes

200 +GHG and SST, +ODS and +GHG, etc. This allows the isolation of the individual forced
201 components of stratospheric temperature change.

202 In the lower stratosphere the SST experiment produces an ensemble-mean warming of
203 about 0.4K over the period from 1979 to 2014 (Figure 2a). This warming is largely due to
204 increasing GHGs aliased into the SSTs (*Karoly and Wu, 2005; Santer et al., 2006*). Figure
205 2b shows that the net effect of increasing GHGs on the global lower stratospheric
206 temperatures is negligible over this specific time period. This net effect is composed of a
207 direct cooling due to radiative effects on the atmosphere (Figure 3a, yellow line) and a
208 warming due to effects mediated by sea surface temperatures (*Folland et al., 1998*). The
209 increase in GHGs also produces an increase in water vapor at 70 hPa (Figure 3c, yellow
210 line) due to the warming of the temperature of the tropopause and the increase in
211 stratospheric methane.

212 Figure 2c shows that most of the observed, slow secular change in lower stratospheric
213 temperature anomalies, which is characterized by steady cooling from 1979 to 1995 and
214 flattening after 1995, is captured by adding the forcing associated with changing ODS
215 concentrations. In the model, the temperature flattening after 1995 is primarily due to the
216 slow-down in ozone depletion with decreasing ODS. The difference in global temperatures
217 in +ODS with respect to +GHG (Fig. 3a, red line) follows the difference in ozone (Fig. 3b,
218 red line). At this altitude, therefore, the concentrations of ODS are the primary determinant
219 of the overall shape of the simulated temperature time series.

220 The strong lower stratospheric warming observed after the volcanic eruptions of El
221 Chichón (1982) and Mt. Pinatubo (1991) is evident in Figure 2d. GEOSSCM overestimates

222 the post-Pinatubo warming with respect to the observations by about 1.5K. This
223 overestimated volcanic warming is a common problem in climate models (*e.g.*, Fig. 1 in
224 *Thompson et al.*, 2012). In the case of GEOSCCM, this is probably due to the use of a fixed
225 aerosol radius of 0.6 μm for aerosol from explosive volcanic eruptions. This value is within
226 the range of observed estimates of the mean particle radius for the aerosol from Mt.
227 Pinatubo, but *Bingen et al.* (2004) showed that the aerosol size changed with time, latitude,
228 and altitude. The inclusion of a time-evolving aerosol size constrains the response to
229 volcanic eruptions by increasing the settling velocities and modifying the aerosol optical
230 properties (*Timmreck et al.*, 2010; *English et al.*, 2013).

231 The lower stratospheric volcanic warming after Mt. Pinatubo lasts about two years, and is
232 followed by a two-year long cooling up to -0.14 K in the ensemble mean with respect to
233 the simulations without volcanic forcing (Figure 3a, green line). This cooling is associated
234 with a depletion of global ozone by about 5% in 1992 (Figure 3b, green line) and an
235 increase in water vapor due to the warming of the tropopause by the volcanic aerosol
236 (Figure 3c, green line). Figure 3a shows that in the model simulations there is no
237 volcanically induced change in global lower stratospheric temperatures between 1986 and
238 1990.

239 The simulation experiment +Sun, which includes all forcings, reproduces the observed
240 low-frequency changes in global temperature anomalies remarkably well, and even
241 captures the observed warming between the El Chichón and Mt. Pinatubo eruptions (Figure
242 2e). Figure 3a (blue line) shows that in the model simulations the solar cycle enhances the
243 cooling of the ensemble mean global temperatures from 1985 to 1986 and the warming
244 from 1989 to 1991, capturing the observed rise in temperatures between the volcanic

245 eruptions. In our simulation the solar cycle creates a small oscillation of the temperature
246 anomalies in phase with its periodicity (Fig. 3a, blue line). This is true in the ensemble
247 mean time series, but the ensemble spread overlaps with zero for the whole simulated time
248 period.

249 **3.2. TEMPERATURE CHANGES IN THE MIDDLE AND UPPER STRATOSPHERE**

250 The GEOSCCM +Sun simulations reliably reproduce many features of the observed global
251 temperature anomalies in the middle (Figure 4e) and upper (Figure 6e, Figure 8e)
252 stratosphere.

253 The SST experiment shows a $\sim 0.1\text{K}$ warming in the SSU1 altitude range (Figure 4a) but
254 no warming at higher altitudes (Figure 6a, Figure 8a). +GHG produces a cooling from 1979
255 to 2014 by 1.2K, 1.7K, and 2.2K in the SSU channels 1, 2, and 3 (Figure 8b), respectively.

256 The increase in GHGs does not produce any trend in global ozone in the middle
257 stratosphere (Figure 5b), but causes an increase in ozone in the upper stratosphere (Figure
258 7b, Figure 9b) due to the slow-down of ozone loss reactions in a colder environment (e.g.
259 *Waugh et al., 2009; Li et al., 2009*). As in the MSU lower stratospheric channel, +GHG
260 also shows an increase in stratospheric water vapor (Figs. 5c, 7c, 9c).

261 The inclusion of estimated observed changes in ODS concentrations (+ODS) strengthens
262 the cooling from 1979 through 2014 in all SSU channels with respect to +GHG and brings
263 the temperature anomalies closer to the observations (Figs. 4c, 6c, 7c). At all levels, the
264 temperature differences between +ODS and +GHG follow the initial decrease and post-
265 1995 flattening of ozone anomalies. This decrease ranges from about 0.1ppm in the middle
266 stratosphere (Figure 5b) to 0.8ppm in the upper stratosphere (Figure 9b). The largest ozone

Global stratospheric temperature changes

267 and temperature differences between +ODS and +GHG are reached in the late 1990s and
268 show a small recovery in the latter part of the simulations. The post-1995 flattening of the
269 global temperature anomalies is not as evident here as in the lower stratosphere (Figure
270 2d), because the influence of ODS on the global temperature with respect to GHGs is
271 smaller in the mid- to upper stratosphere.

272 The simulated stair-step behavior of the global stratospheric temperature anomalies in the
273 SSU channels is primarily due to GHG-induced cooling and the superimposed modulation
274 by the solar cycle. Between 1993 and 1995 the volcanically induced ozone depletion and
275 water vapor increase cause a cooling of similar magnitude as the one associated to the solar
276 cycle, anticipating the onset of the flattening of temperature anomalies between the mid
277 1990s and the mid 2000s.

278 As in the lower stratosphere, the volcanic forcing produces a warming in 1982-1983 and
279 1991-1993 (Figs. 4d, 6d, 8d). In these altitude ranges, GEOSCCM reproduces the
280 magnitude of the volcanic warming with respect to observations. Again, a cooling with
281 respect to +ODS lasting until the late 1990s follows the volcanic warming associated with
282 the Mt. Pinatubo eruption. This cooling is present in all SSU channels (Figs. 5a, 7a, 9a)
283 and is associated with an increase in stratospheric water vapor (Figs. 5c, 7c, 9c). At these
284 altitudes, there is no significant ozone depletion associated with the eruption of Mt.
285 Pinatubo (Figs. 5b, 7b, 9b).

286 In all three SSU channels, the forcing associated with the solar cycle contributes not only
287 to the flattening of temperature anomalies between 1985 and 1991, as in MSU channel 4,
288 but also to the post-1995 flattening of the global stratospheric temperatures (Figs. 4e, 6e,

289 8e). This modulation of the temperature anomaly (Figs. 5a, 7a, 9a) is associated to solar-
290 induced modulation of ozone concentrations (Figs. 5b, 7b, 9b).

291 **3.3 TEMPERATURE TRENDS**

292 We calculated the global temperature trends for the periods from January 1979 to
293 December 1997 and January 2000 to December 2011 and over the whole available time
294 series , *i.e.* 1979-2014 for MSU and model simulations, and 1979-2011 for SSU (Fig. 10).
295 The first two periods are chosen to match the periods used in the 2014 WMO Assessment
296 on Ozone Depletion (*Pawson et al., 2014*). The upper panels of Fig. 10 show the
297 temperature trends in the observations and in the ensemble mean of the experiment with
298 full forcings (+Sun). Trends are calculated from the deseasonalized monthly mean
299 temperatures by minimizing the least-squared deviations. The 95% confidence intervals
300 take into account the autocorrelation of the residuals following *Santer et al. (2000)*. The
301 resulting trends and respective confidence intervals are reported in Table 2. The large lower
302 stratospheric volcanic warming, overestimated in GEOSCCM with respect to the
303 observations, causes the very large confidence intervals over 1979-1997 (Fig. 10a).

304 The lower panels of Fig. 10 show the trends of the ensemble mean-differences between
305 successive pairs of simulations, in order to isolate the contributions of each forcing agent
306 to the total simulated temperature trends. In the middle and upper stratosphere the cooling
307 caused by GHGs is the dominant contribution during all time periods considered. In our
308 simulations the GHG associated cooling goes from about -0.4 K/decade in SSU1 to about
309 0.6 K/decade in SSU3. From 2005 to present, however, these cooling trends could be
310 underestimated, since the RCP4.5 scenario used in our simulations prescribes GHG
311 emissions lower than observed from 2005 to 2014.

Global stratospheric temperature changes

312 Increasing ODS concentrations produce an additional cooling only over the 1979-1997
313 time period from -0.2 K/decade in SSU1 to -0.49 K/decade in SSU3. After 2000,
314 decreasing ODS concentrations cause a positive temperature trends in SSU2 and SSU3,
315 and do not contribute in a statistically significant way to the temperature trends in the MSU
316 and SSU1 altitude ranges. Over the whole time series, the GHG and ODS contributions to
317 the lower stratospheric temperature trends are of the same magnitude, while in the middle
318 and upper stratosphere the ODS contribution is between 20% and 31% of the GHG
319 contribution in the SSU1 and SSU3 altitude ranges, respectively.

320 We expect some nonlinearities to arise when adding the effects of ODS to GHGs. Ozone
321 loss is reduced in a colder environment, so that the GHG-induced cooling limits ozone
322 depletion and the subsequent stratospheric cooling. These nonlinear effects are included in
323 our individual simulations because ozone, temperature, and dynamics are coupled to each
324 other, but the use of differences between simulations to quantify the effects of single
325 forcings relies on the assumption that these effects add linearly. *Meul et al. (2015)* showed
326 that nonlinearity significantly weakens ODS-related cooling in the tropical upper
327 troposphere and in the lower to middle stratosphere at southern midlatitudes, inducing
328 temperature changes between 1960 and 2000 of up to 0.4K. This corresponds to a
329 0.1K/decade trend. In these two regions our simulated ODS-induced temperature trend
330 over the 1979-1997 is 0.6K/decade and 0.4K/decade, respectively (not shown).
331 Considering the 0.1K/decade calculated by *Meul et al. (2015)*, our estimate of the ODS
332 related cooling could be locally underestimated by 16% and 25% in the tropical upper
333 stratosphere and lower stratosphere at southern midlatitudes, respectively.

334 In our simulations volcanic eruptions cause a warming trend over the 2000-2011 period,
335 which is statistically significant only in the SSU channels. This period is characterized by
336 a series of relatively small volcanic eruptions that reached the stratosphere and increased
337 stratospheric aerosol concentrations (*Vernier et al., 2011; Neely et al., 2013*). The large
338 volcanic perturbations of El Chichón and Mt. Pinatubo produce a statistically significant
339 cooling trend only over 1979-1997 in the upper stratosphere (SSU3). There, the increase
340 in stratospheric water vapor after Mt. Pinatubo produces an additional cooling from 1993
341 to 1996 (Fig. 9), resulting in a significant cooling trend of -0.11 K/decade. However, the
342 overestimation of the lower stratospheric volcanic warming immediately following the
343 eruptions might have led to an overestimation of the water vapor entering the stratosphere
344 after the eruption of Mt. Pinatubo and therefore to a too large volcanic cooling in the upper
345 stratosphere. Over the whole time series, volcanic eruptions did not contribute to the
346 simulated temperature trends.

347 **4. CONCLUSIONS**

348 In our simulations the cooling of the stratosphere from 1979 to present is driven by changes
349 in ODS and GHG concentrations in the lower stratosphere and mostly by changes in GHG
350 concentrations in the middle and upper stratosphere, in agreement with previous studies
351 (*e.g. Stolarski et al. 2010; Gillett et al., 2011*). Changing ODS concentrations also had an
352 impact on the temperature trends, significantly adding to the GHG-associated cooling up
353 to 1997. After 2000, with the application of the Montreal Protocol, decreasing ODS
354 concentrations produced a warming trend in the upper stratosphere.

Global stratospheric temperature changes

355 In our simulations volcanic eruptions did not have a statistically significant impact on the
356 simulated temperature trends in the lower stratosphere, where the confidence intervals on
357 the simulated trends are large because of the overestimation of the volcanic warming. On
358 the other hand, volcanic eruptions produced a statistically significant warming in the SSU
359 channels over the 2000-2011 period, period characterized by a series of smaller volcanic
360 eruptions that reached the stratosphere (Vernier et al., 2011). Trends calculated over the
361 whole simulated temperature time series show that in our model the solar cycle did not
362 impact the stratospheric temperature trends from 1979 to present.

363 In our simulations the flattening of the global temperature anomalies between the El
364 Chichón and Mount Pinatubo eruptions is an effect of the solar cycle both in the MSU and
365 in the SSU channels. In the MSU channel, however, the effects of the solar cycle are very
366 noisy, and the ensemble spread overlaps with zero. In the mid 1990s, the eruption of Mt.
367 Pinatubo induced an initial warming followed by a cooling of stratospheric temperatures
368 associated to the enhanced ozone depletion and increased stratospheric water vapor
369 concentrations, causing the abrupt step. The decrease in ODS concentrations and the
370 subsequent decrease in ozone depletion caused the flattening of the lower stratospheric
371 temperature anomalies after 1998, as suggested by *Ferraro et al. (1995)*. In the middle and
372 upper stratosphere, the solar cycle concurred with the volcanic cooling to create the post-
373 1995 temperature flattening until 1998. After 1998 it is the onset of a solar maximum that
374 kept the temperature anomalies from decreasing further. The characteristic stair step
375 pattern in the temperature anomalies is therefore caused by a combination of all the forcings
376 acting on the stratospheric temperatures.

377 **Acknowledgments**

378 The authors would like to thank D. Seidel, L. Oman, and P. Newman for useful discussions,
379 and C. McLandress for providing the AMSU/SSU temperature data. We also thank the
380 three reviewers for their comments. The model simulations were performed at the NASA
381 Center for Climate Simulation. W. H. S. is funded for this work by a grant from NASA's
382 Living With a Star program. L. M. P. and D. W. W. are funded, in part, by a grant from the
383 U.S. National Science Foundation. The MSU data record is available at
384 <http://www.remss.com/measurements/upper-air-temperature>. The simulated temperature
385 records are available upon request to the corresponding author.

386

387 **References**

388 Angell, J. K. (1997). Stratospheric warming due to Agung, El Chichón, and Pinatubo
389 taking into account the quasi-biennial oscillation. *J. Geophys. Res.*, *102*(D8), 9479–9485.
390 doi: 10.1029/96JD03588

391 Aquila, V., Oman, L. D., Stolarski, R. S., Colarco, P. R., and Newman, P. A. (2012).
392 Dispersion of the volcanic sulfate cloud from a Mount Pinatubo–like eruption. *J.*
393 *Geophys. Res.*, *117*, D06216. doi:10.1029/2011JD016968

394 Aquila, V., Oman, L. D., Stolarski, R., Douglass, A. R., and Newman, P. A. (2013).
395 The Response of Ozone and Nitrogen Dioxide to the Eruption of Mt. Pinatubo at
396 Southern and Northern Midlatitudes. *J. Atmos. Sci.*, *70*(3), 894–900. doi:10.1175/JAS-D-
397 12-0143.1

398 Bingen, C., Fussen, D., and Vanhellemont, F. (2004). A global climatology of
399 stratospheric aerosol size distribution parameters derived from SAGE II data over the
400 period 1984-2000: 2. Reference data. *J. Geophys. Res.* *109*(D6), D06202.
401 doi:10.1029/2003JD003511

402 Carn, S. A., Yang, K., Prata, A. J., and Krotkov, N. A. (2015). Extending the long-
403 term record of volcanic SO₂ emissions with the Ozone Mapping and Profiler Suite
404 (OMPS) Nadir Mapper. *Geophys. Res. Lett.*, *42*. doi:10.1002/2014GL062437

405 Chin, M., Rood, R. B., Lin, S.-J., and Müller, J.-F. (2000). Atmospheric sulfur cycle
406 simulated in the global model GOCART: Model description and global properties. *J.*
407 *Geophys. Res.*, *105*(D20), 24671–24687. doi:10.1029/2000JD900384

408 Coddington, O., Lean, J. L., Pilewskie, P., Snow, M., and Lindholm, D. (2015). A
409 solar irradiance climate data record. *Bull. Amer. Meteorol. Soc.* Doi: 10.1175/BAMS-D-
410 14-00265.1

411 Colarco, P., Da Silva, A., Chin, M., and Diehl, T. (2010). Online simulations of
412 global aerosol distributions in the NASA GEOS-4 model and comparisons to satellite and
413 ground-based aerosol optical depth. *J. Geophys. Res.*, *115*(D14), D14207.
414 doi:10.1029/2009JD012820

415 Diehl, T., Heil, A., Chin, M., Pan, X., Streets, D., Schultz, M., and Kinne, S. (2012).
416 Anthropogenic, biomass burning, and volcanic emissions of black carbon, organic
417 carbon, and SO₂ from 1980 to 2010 for hindcast model experiments. *Atmos. Chem. Phys.*
418 *Discuss.*, *12*(9), 24895–24954. doi:10.5194/acpd-12-24895-2012

419 Douglass, A. R., R. S. Stolarski, S. E. Strahan, and L. D. Oman (2012),
420 Understanding differences in upper stratospheric ozone response to changes in chlorine
421 and temperature as computed using CCMVal-2 models, *J. Geophys. Res.*, 117, D16306,
422 doi:10.1029/2012JD017483.

423 English, J. M., Toon, O. B., and Mills, M. J. (2013). Microphysical simulations of
424 large volcanic eruptions: Pinatubo and Toba. *J. Geophys. Res.*, 118, 1-16.
425 doi:10.1002/jgrd.50196

426 Eyring, V., Butchart, N., Waugh, D. W., Akiyoshi, H., Austin, J., Bekki, S., et al.
427 (2006). Assessment of temperature, trace species, and ozone in chemistry-climate model
428 simulations of the recent past. *J. Geophys. Res.*, 111(D22). doi:10.1029/2006JD007327

429 Ferraro, A. J., Collins, M., and Lambert, F. H. (2015). A hiatus in the stratosphere?
430 *Nature Climate Change*, 5(6), 497–498. doi:10.1038/nclimate2624

431 Folland, C. K., Sexton, D. M. H., Karoly, D. J., Johnson, C. E., Rowell, D. P., and
432 Parker, D. E. (1998). Influences of anthropogenic and oceanic forcing on recent climate
433 change. *Geophys. Res. Lett.*, 25(3), 353–356. Doi:10.1029/97GL03701

434 Granier, C., Bessagnet, B., Bond, T., D'Angiola, A., Denier van der Gon, H., Frost,
435 G. J., et al. (2011). Evolution of anthropogenic and biomass burning emissions of air
436 pollutants at global and regional scales during the 1980–2010 period. *Climatic Change*,
437 109(1-2), 163–190. doi: 10.1007/s10584-011-0154-1

438 Gray, L. J., Rumbold, S. T., and Shine, K. P. (2009). Stratospheric Temperature and
439 Radiative Forcing Response to 11-Year Solar Cycle Changes in Irradiance and Ozone. *J.*
440 *Atmos. Sci.*, *66*, 2402–2417. doi:10.1175/2009JAS2866.1

441 Jones, G. S., Tett, S. F. B., and Stott, P. A. (2003). Causes of atmospheric
442 temperature change 1960–2000: A combined attribution analysis. *Geophys. Res. Lett.*,
443 *30*(5), 1228. Doi: 10.1029/2002GL016377

444 Karoly, D. J., and Wu, Q. (2005). Detection of Regional Surface Temperature
445 Trends. *J. Clim.*, *18*(21), 4337–4343. Doi:10.1175/JCLI3565.1

446 Lean, J. (2000): Evolution of the Sun’s Spectral Irradiance Since the Maunder
447 Minimum, *Geophys. Res. Lett.*, *27*, 2425–2428. doi:10.1029/2000GL000043

448 Li, F., Stolarski, R. S., and Newman, P. A. (2009). Stratospheric ozone in the post-
449 CFC era. *Atmos. Chem. Phys.*, *9*, 2207–2213. Doi:10.5194/acp-9- 2207-2009

450 Liang, Q., R. S. Stolarski, S. R. Kawa, J. E. Nielsen, J. M. Rodriguez, D. R. Blake,
451 E. L. Atlas, and L. E. Ott (2010), Finding the missing stratospheric Br_y: A global
452 modeling study of CHBr₃ and CH₂Br₂, *Atmos. Chem. Phys.*, *10*, 2269–2286.
453 doi:10.5194/acp-10-2269-2010

454 McLandress, C., T. G. Shepherd, A. I. Jonsson, T. von Clarmann, and B. Funke
455 (2015). A method for merging nadir-sounding climate records, with an application to the
456 global-mean stratospheric temperature data sets from SSU and AMSU. *Atmos. Chem.*
457 *Phys.*, *15*(16), 9271–9284. doi: 10.5194/acp-15-9271-2015

458 Mears, C. A. and F. J. Wentz, (2009). Construction of the Remote Sensing Systems
459 V3.2 Atmospheric Temperature Records From the MSU and AMSU Microwave
460 Sounders, *J. Atmos. Ocean. Tech.*, 26, 1040-1056. doi: 0.1175/2008JTECHA1176.1

461 Meinshausen, M., S. J. Smith, K. V. Calvin, J. S. Daniel, M. L. T. Kainuma, J.-F.
462 Lamarque, K. Matsumoto, S. A. Montzka, S. C. B. Raper, K. Riahi, A. M. Thomson, G.
463 J. M. Velders and D. van Vuuren (2011). The RCP Greenhouse Gas Concentrations and
464 their Extension from 1765 to 2300. *Climatic Change*, 109(1-2), 213-241. doi:
465 10.1007/s10584-011-0156-z

466 Meul, S., Oberländer-Hayn, S., Abalichin, J., and Langematz, U. (2015). Nonlinear
467 response of modelled stratospheric ozone to changes in greenhouse gases and ozone
468 depleting substances in the recent past. *Atmos. Chem. Phys.*, 15(12), 6897–6911.
469 Doi:10.5194/acp-15-6897-2015

470 Molod, A., L. Takacs, M. Suarez, J. Bacmeister, I.-S. Song, and A. Eichmann
471 (2012), The GEOS–5 atmospheric general circulation model: Mean climate and
472 development from MERRA to Fortuna, Technical Report Series on Global Modeling and
473 Data Assimilation, vol. 28. [<http://gmao.gsfc.nasa.gov/pubs/docs/Molod484.pdf>.]

474 Nash, J., and Forrester, G. F. (1986). Long-term monitoring of stratospheric
475 temperature trends using radiance measurements obtained by TIROS-N series of NOAA
476 spacecraft. *Adv. Space Res.*, 6(10), 37–44. doi:10.1016/0273-1177(86)90455-2

477 Nash, J., and R. Saunders (2015). A review of Stratospheric Sounding Unit radiance
478 observations for climate trends and reanalyses. *Q. J. Meteorol. Soc.*, 141(691), 2103–
479 2113. <http://doi.org/10.1002/qj.2505>

Global stratospheric temperature changes

480 Neely, R. R., III, Toon, O. B., Solomon, S., Vernier, J. P., Alvarez, C., English, J.
481 M., et al. (2013). Recent anthropogenic increases in SO₂ from Asia have minimal impact
482 on stratospheric aerosol. *Geophys. Res. Lett.*, *40*(5), 999–1004. [doi:10.1002/grl.50263](https://doi.org/10.1002/grl.50263)

483 Newman, P. A., Daniel, J. S., Waugh, D. W., and Nash, E. (2007). A new
484 formulation of equivalent effective stratospheric chlorine (EESC). *Atmos. Chem. Phys.*, *7*,
485 4537–4552. doi:10.5194/acp-7-4537-2007

486 Oman, L. D., and Douglass, A. R. (2014). Improvements in Total Column Ozone in
487 GEOSCCM and Comparisons with a New Ozone Depleting Substances Scenario. *J.*
488 *Geophys. Res.*, *119*, 5613–5624. doi:10.1002/2014JD021590

489 Pawson, S., Labitzke, K., and Leder, S. (1998). Stepwise changes in stratospheric
490 temperature. *Geophys. Res. Lett.*, *25*(12), 2157–2160. doi:10.1029/98GL51534

491 Pawson, S., Stolarski, R. S., Douglass, A. R., Newman, P. A., Nielsen, J. E., Frith, S.
492 M., and Gupta, M. L. (2008). Goddard Earth Observing System chemistry-climate model
493 simulations of stratospheric ozone-temperature coupling between 1950 and 2005. *J.*
494 *Geophys. Res.*, *113*(D12), D12103. doi:10.1029/2007JD009511

495 Pawson, S., Steinbrecht, W., Charlton-Perez, A. J., Fujiwara, M., Karpechko, A. Y.,
496 Petropavlovskikh, I., et al. (2014). Update on Global Ozone: Past, Present, and Future. In
497 *Scientific Assessment of Ozone Depletion: 2014*. Global Ozone Research and Monitoring
498 Project.

Global stratospheric temperature changes

- 499 Ramaswamy, V., and Schwarzkopf, M. (2002). Effects of ozone and well-mixed
500 gases on annual-mean stratospheric temperature trends. *Geophys. Res. Lett.*, 29(22),
501 2064. doi:10.1029/2002GL015141
- 502 Ramaswamy, V., Schwarzkopf, M. D., Randel, W. J., Santer, B. D., Soden, B. J.,
503 and Stenchikov, G. L. (2006). Anthropogenic and Natural Influences in the Evolution of
504 Lower Stratospheric Cooling. *Science*, 311(5764), 1138–1141.
505 doi:10.1126/science.1122587
- 506 Randel, W. J., Shine, K. P., Austin, J., Barnett, J., Claud, C., Gillett, N., et al. (2009).
507 An update of observed stratospheric temperature trends. *J. Geophys. Res.*, 114, D02107.
508 doi:10.1029/2008JD010421
- 509 Rayner, N. A., P. Brohan, D. E. Parker, C. K. Folland, J. J. Kennedy, M. Vanicek, T.
510 Ansell and S. F. B. Tett, 2006: Improved analyses of changes and uncertainties in sea
511 surface temperature measured in situ since the mid-nineteenth century: the HadSST2 data
512 set. *J. Clim.*, 19(3), 446-469. doi: <http://dx.doi.org/10.1175/JCLI3637.1>
- 513 Rienecker, M. M., et al. (2008), The GEOS-5 data assimilation system -
514 Documentation of versions 5.0.1, 5.1.0, and 5.2.0. Technical Report Series on Global
515 Modeling and Data Assimilation, 27.
- 516 Santer, B. D., Wigley, T. M. L., Boyle, J. S., Gaffen, D. J., Hnilo, J. J., Nychka, D.,
517 et al. (2000). Statistical significance of trends and trend differences in layer-average
518 atmospheric temperature time series. *J. Geophys. Res.*, 105(D6), 7337–7356. doi:
519 10.1029/1999JD901105

Global stratospheric temperature changes

520 Santer, B. D., Sausen, R., Wigley, T. M. L., Boyle, J. S., AchutaRao, K. M.,
521 Doutriaux, C., et al. (2003). Behavior of tropopause height and atmospheric temperature
522 in models, reanalyses, and observations: Decadal changes. *J. Geophys. Res.*, *108*(D1),
523 4002. doi: [10.1029/2002JD002258](https://doi.org/10.1029/2002JD002258)

524 Santer, B. D., Wigley, T. M. L., Gleckler, P. J., Bonfils, C., Wehner, M. F.,
525 AchutaRao, K., et al. (2006). Forced and unforced ocean temperature changes in Atlantic
526 and Pacific tropical cyclogenesis regions. *P. Natl. Acad. Sci. USA*, *103*(38), 13905–
527 13910. <http://doi.org/10.1073/pnas.0602861103>

528 Santer, B. D., Painter, J. F., Bonfils, C., Mears, C. A., Solomon, S., Wigley, T. M.
529 L., et al. (2013). Human and natural influences on the changing thermal structure of the
530 atmosphere. *Proc. Natl. Acad. Sci. U.S.A.*, *110*(43), 17235–17240.
531 Doi:10.1073/pnas.1305332110.

532 Santer, B. D., Solomon, S., Bonfils, C., Zelinka, M. D., Painter, J. F., Beltran, F., et
533 al. (2015). Observed multivariable signals of late 20th and early 21st century volcanic
534 activity. *Geophys. Res. Lett.*, *42*(2), 500–509. Doi: 10.1002/2014GL062366

535 Seidel, D. J., Gillett, N. P., Lanzante, J. R., Shine, K. P., and Thorne, P. W. (2011).
536 Stratospheric temperature trends: our evolving understanding. *WIREs: Climate Change*,
537 *2*, 592–616. doi:10.1002/wcc.125

538 Shepherd, T. G., and Jonsson, A. I. (2008). On the attribution of stratospheric ozone
539 and temperature changes to changes in ozone-depleting substances and well-mixed
540 greenhouse gases. *Atmos. Chem. Phys.*, *8*(5), 1435–1444. doi:10.5194/acp-8-1435-2008

541 SPARC Chemistry-Climate Model Validation (CCMVal) (2010), SPARC CCMVal
542 report on the evaluation of chemistry-climate models, SPARC Rep. 5, WCRP-132,
543 WMO/TD-No. 1526, edited by V. Eyring et al. [Available at
544 <http://www.atmosph.physics.utoronto.ca/SPARC.>]

545 Stolarski, R. S., Douglass, A. R., Newman, P. A., Pawson, S., and Schoeberl, M. R.
546 (2010). Relative Contribution of Greenhouse Gases and Ozone-Depleting Substances to
547 Temperature Trends in the Stratosphere: A Chemistry–Climate Model Study. *J. Clim.*,
548 23, 28–42. doi:10.1175/2009JCLI2955.1

549 Strahan, S. E., et al. (2011), Using transport diagnostics to understand chemistry
550 climate model ozone simulations, *J. Geophys. Res.*, 116, D17302,
551 doi:10.1029/2010JD015360.

552 Swartz, W. H., R. S. Stolarski, L. D. Oman, E. L. Fleming, and C. H. Jackman
553 (2012), Middle atmosphere response to different descriptions of the 11-yr solar cycle
554 in spectral irradiance in a chemistry–climate model, *Atmos. Chem. Phys.*, 12, 5937–
555 5948, doi:10.5194/acp-12-5937-2012.

556 Tie, X., and Brasseur, G. (1995). The response of stratospheric ozone to volcanic
557 eruptions: Sensitivity to atmospheric chlorine loading. *Geophys. Res. Lett.*, 22(22), 3035–
558 3038. Doi: 10.1029/95GL03057

559 Thompson, D. W. J., and Solomon, S. (2009). Understanding Recent Stratospheric
560 Climate Change. *J. Clim.*, 22(8), 1934–1943. doi:10.1175/2008JCLI2482.1

Global stratospheric temperature changes

561 Thompson, D. W. J., Seidel, D. J., Randel, W. J., Zou, C.-Z., Butler, A. H., Mears,
562 C., et al. (2012). The mystery of recent stratospheric temperature trends. *Nature Climate*
563 *Change*, 491(7426), 692–697. doi:10.1038/nature11579

564 Timmreck, C., Graf, H.-F., Lorenz, S. J., Niemeier, U., Zanchettin, D., Matei, D., et
565 al. (2010). Aerosol size confines climate response to volcanic super-eruptions. *Geophys.*
566 *Res. Lett.*, 37, L24705. Doi: 10.1029/2010GL045464

567 Vernier, J. P., Thomason, L. W., Pommereau, J. P., Bourassa, A., Pelon, J., Garnier,
568 A., et al. (2011). Major influence of tropical volcanic eruptions on the stratospheric
569 aerosol layer during the last decade. *Geophys. Res. Lett.*, 38(12). Doi:
570 10.1029/2011GL047563

571 Wang, L., Zou, C.-Z. and Qian, H. Construction of stratospheric temperature data
572 records from stratospheric sounding units. *J. Clim.* 25, 2931–2946 (2012). doi:
573 10.1175/JCLI-D-11-00350.1

574 Waugh, D. W., Oman, L., Kawa, S. R., Stolarski, R. S., Pawson, S., Douglass, A. R.,
575 et al. (2009). Impacts of climate change on stratospheric ozone recovery. *Geophys. Res.*
576 *Lett.*, 36(3), L03805–6. Doi:10.1029/2008GL036223

577 WMO (2010), Scientific Assessment of Ozone Depletion: 2010, Global Ozone
578 Research and Monitoring Project – Report No. 55, 416 pp., Geneva, Switzerland.

579 Zou, C.-Z., Qian, H., Wang, W., Wang, L., and Long, C. (2014). Recalibration and
580 merging of SSU observations for stratospheric temperature trend studies. *J. Geophys.*
581 *Res.*, 119(23). doi:10.1002/2014JD021603

582 **Tables**

583 Table 1: Forcings applied in the simulation experiments performed for this study.

Forcing	Reference	Experiment name				
		SST	+GHG	+ODS	+Volc	+Sun
SST	<i>Rayner et al. (2006)</i>	X				
GHGs	<i>Meinhausen et al. (2007)</i>	X	X			
ODS	<i>WMO (2010)</i>	X	X	X		
Volcanic eruptions	<i>Diehl et al. (2012), Carn et al. (2014)</i>	X	X	X	X	
Solar cycle	<i>Lean (2000)</i>	X	X	X	X	X

584

585

Global stratospheric temperature changes

586 Table 2: Global temperature trends in observations and +Sun simulation in K/decade and
 587 respective 95% confidence intervals, calculated using monthly mean anomalies. Trends in
 588 italics are not statistically significant. These values are plotted in Fig.10.

MSU (15km-20km)

	1979-1997	2000-2011	Whole time series
+Sun	-	<i>0.07±0.18</i>	<i>-0.14±0.30</i>
	<i>0.26±1.59</i>		
Observations	-	<i>-0.09±0.26</i>	<i>-0.27±0.15</i>
	<i>0.41±0.65</i>		
Single Forcings			
SSTs	0.06±0.05	0.15±0.08	0.09±0.02
GHGs	-	<i>-0.09±0.09</i>	<i>-0.09±0.02</i>
	0.10±0.05		
ODS	-	<i>-0.03±0.14</i>	<i>-0.09±0.03</i>
	0.20±0.04		
Volcanoes	<i>0.03±1.66</i>	<i>0.07±0.14</i>	<i>-0.05±0.27</i>
Solar cycle	-	<i>-0.02±0.14</i>	<i>0.00±0.03</i>
	<i>0.06±0.07</i>		

Global stratospheric temperature changes

SSU1 (25km-35km)

	1979-1997	2000-2011	Whole time series
+Sun	-	-0.43±0.28	-0.49±0.21
	<i>0.78±0.79</i>		
Observations	-	-0.45±0.13	-0.63±0.12
	<i>0.88±0.33</i>		
Single Forcings			
SSTs	<i>0.02±0.03</i>	<i>0.04±0.05</i>	<i>0.04±0.01</i>
GHGs	-	-0.42±0.05	-0.41±0.01
	<i>0.40±0.03</i>		
ODS	-	<i>0.01±0.07</i>	-0.08±0.02
	<i>0.20±0.02</i>		
Volcanoes	-	0.09±0.08	-0.03±0.13
	<i>0.08±0.71</i>		
Solar cycle	-	-0.16±0.25	-0.01±0.05
	<i>0.12±0.12</i>		

SSU2 (35km-45km)

Global stratospheric temperature changes

	1979-1997	2000-2011	Whole time series
+Sun	-	-0.64±0.39	-0.68±0.26
	1.12±0.58		
Observations	-	-0.54±0.13	-0.70±0.13
	1.07±0.31		
Single Forcings			
SSTs	<i>0.00±0.03</i>	<i>0.00±0.05</i>	<i>0.01±0.01</i>
GHGs	-	-0.55±0.04	-0.53±0.01
	0.51±0.02		
ODS	-	0.07±0.05	-0.13±0.03
	0.34±0.02		
Volcanoes	-	0.09±0.05	-0.01±0.06
	0.09±0.25		
Solar cycle	-	-0.25±0.42	-0.02±0.10
	0.18±0.24		
SSU3 (40km-50km)			
	1979-1997	2000-2011	Whole time series

Global stratospheric temperature changes

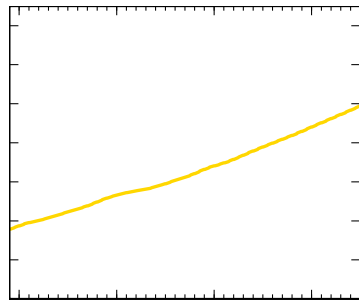
+Sun	-	-0.76±0.61	-0.84±0.46
		1.47±0.68	
<hr/>			
Observations	-	-0.65±0.14	-0.78±0.16
		1.15±0.51	
<hr/>			
Single Forcings			
<hr/>			
SSTs	-	-0.03±0.04	-0.01±0.01
		0.02±0.02	
<hr/>			
GHGs	-	-0.61±0.04	-0.61±0.01
		0.60±0.02	
<hr/>			
ODS	-	0.11±0.05	-0.19±0.05
		0.49±0.02	
<hr/>			
Volcanoes	-	0.10±0.04	0.00±0.03
		0.11±0.10	
<hr/>			
Solar cycle	-	-0.32±0.60	-0.03±0.15
		0.24±0.38	

589

590

591

592 **Figures**



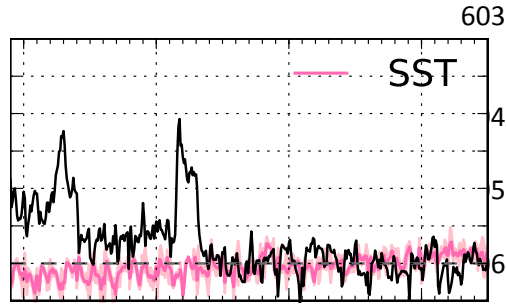
)

c)

3
4
5
5
7
8
9
0
1
2

Figure 1: Forcing applied in the simulations. a) Atmospheric concentrations of CO₂; b) equivalent effective stratospheric chlorine (EESC, Newman *et al.*, 2007); c) ensemble mean of the aerosol optical thickness from explosive volcanic eruptions, resulting from prescribed injections of volcanic SO₂; d) total solar irradiance.

Global stratospheric temperature changes



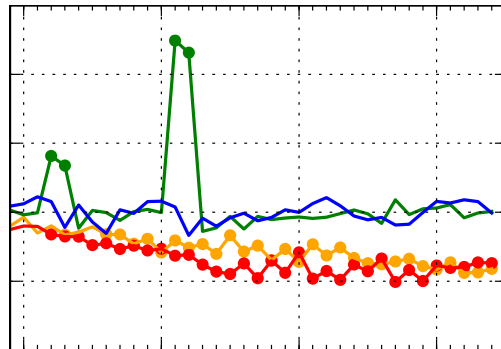
b)

c)

d)

e)

Figure 2: Stratospheric temperature anomalies with respect to the 1995-2011 climatological monthly means as calculated from MSU observations (black lines) and model simulations. Model results are weighted with the MSU channel 4 weighting function, which covers the 15km to 25 km altitude range. Anomalies are calculated over 75°S-75°N. The solid colored lines show the model ensemble means, and the shaded areas the ensemble spread.



620

621

622

623

624

625

626

627

628

629

630

631

632

633

634

635

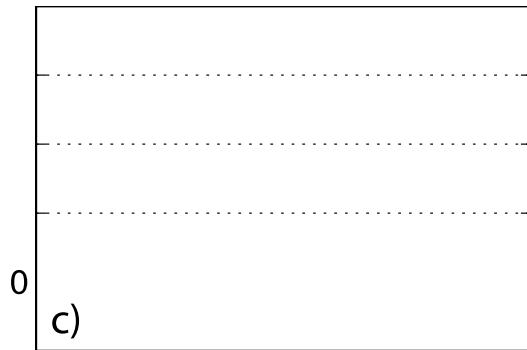
636

637

638

639

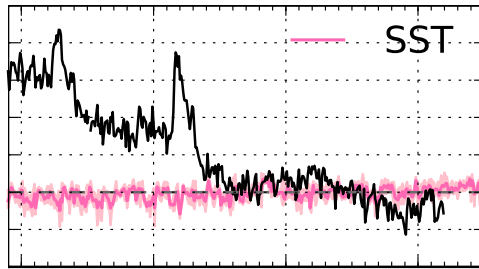
Figure 3: 75°S-75°N annual mean temperature changes in the MSU channel 4 altitude range (15km to 25km - upper panel), and 60°S-60°N ozone (middle panel) and water vapor (lower panel) annual mean anomalies at 70 hPa due to each forcing agent, calculated as the ensemble mean differences between (yellow) +GHG and SST, (red) +ODS and +GHG, (green) +Volc and +ODS, and (blue) +Sun and +Volc. Lines indicate the ensemble means, and the dots mark years where the simulated ensemble spread does not



640 **overlap with zero (all ensemble members show a response of the same sign).**

Global stratospheric temperature changes

641

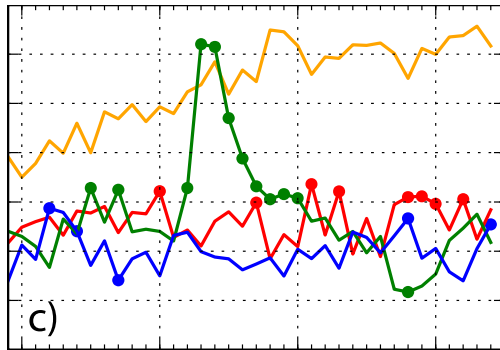
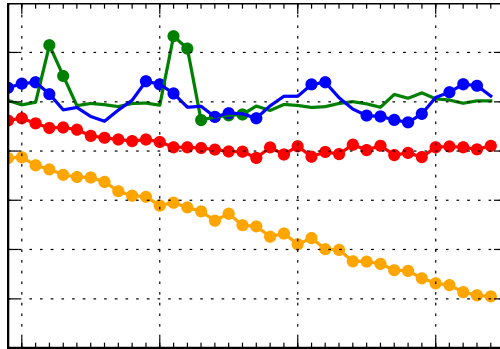


c)

d)

e)

642 **Figure 4: As Fig.2 but for SSU1 (25km-35km).**



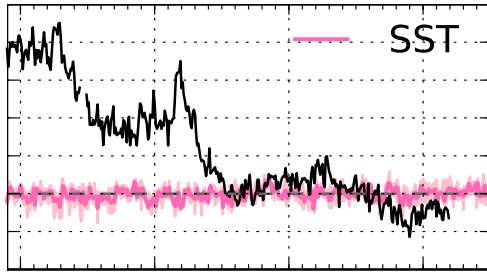
643

644 **Figure 5: As Fig.3, but temperature differences are calculated for SSU1 (25km-**

645 **35km), and ozone and water vapor differences at 20 hPa.**

Global stratospheric temperature changes

646

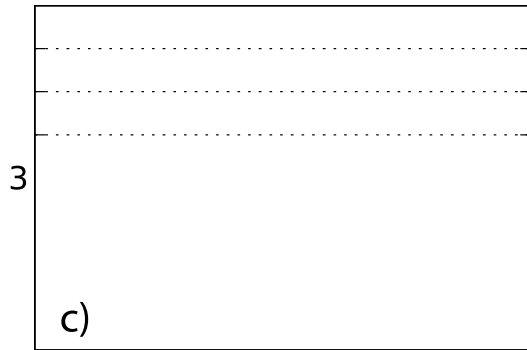
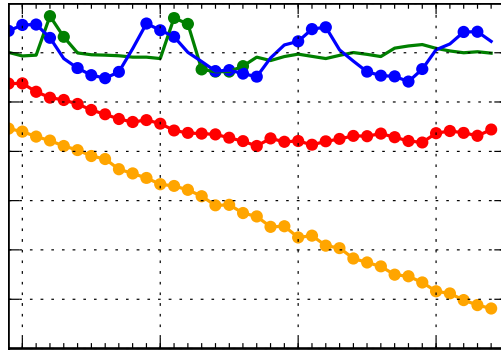


c)

d)

e)

647 **Figure 6: As Fig.2 but for SSU2 (35km-45km).**



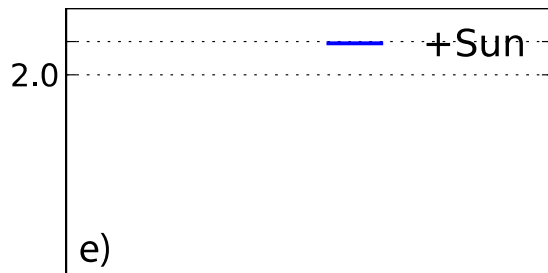
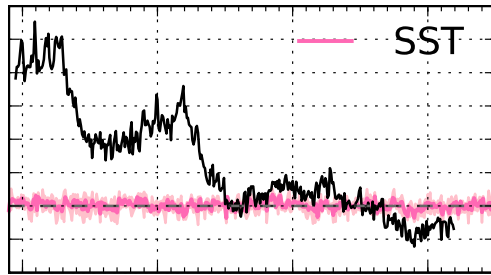
648

649 **Figure 7: As Figure 3, but temperature differences are calculated for SSU2 (35km-**

650 **45km), and ozone and water vapor differences at 5 hPa.**

Global stratospheric temperature changes

651

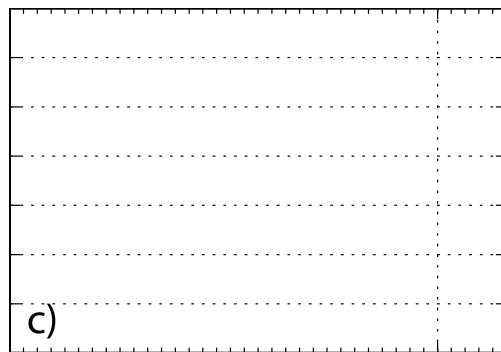
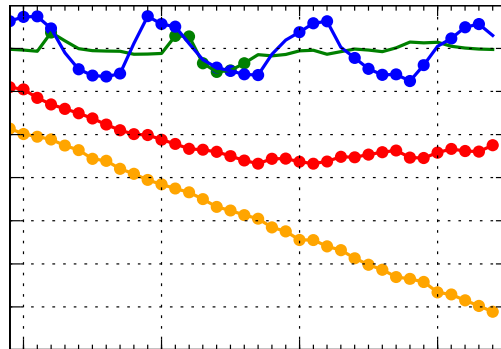


Global stratospheric temperature changes

652 **Figure 8: As Fig.2 but for SSU3 (40km-50km).**

653

Global stratospheric temperature changes



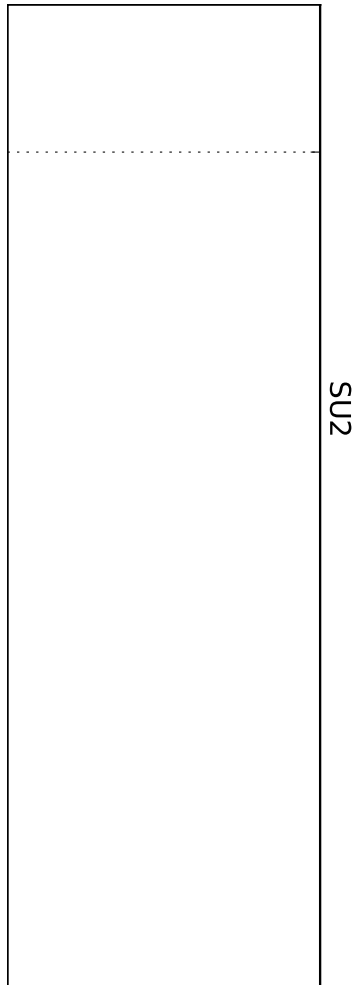
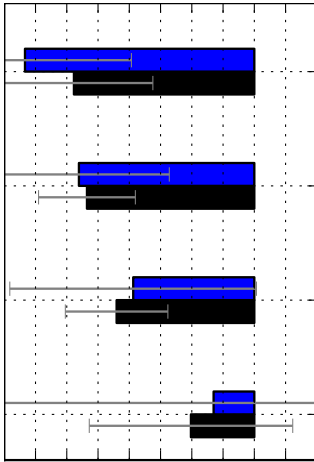
0

654

655 **Figure 9: As Fig.3, but temperature differences are calculated for SSU3 (40km-**

656 **50km), and ozone and water vapor differences at 2 hPa.**

Global stratospheric temperature changes



658 **Figure 10: Global temperature trends for the periods from (a, d) January 1979 to**
659 **December 1997 and (b, e) January 2000 to December 2011, and (c, f) over the whole**
660 **available time series (1979-2011 for SSU, 1979-2014 for MSU and simulations). The**
661 **upper panels show trends from observations (black) and the +Sun ensemble mean**
662 **(blue). The lower panels show the contributions of each forcing agents to the**
663 **temperature trends, calculated from the ensemble mean difference time series**
664 **between (yellow) +GHG and SST, (red) +ODS and +GHG, (green) +Volc and +ODS,**
665 **and (blue) +Sun and +Volc. The trend due to SSTs (pink) is calculated over the**
666 **ensemble mean temperature time series of the SST simulations. Trends are**
667 **calculated using monthly mean temperature anomalies. Whiskers show the 95%**
668 **confidence interval.**

669